Med Biol Eng Comput (2015) 53:879–887
DOI 10.1007/s11517-015-1296-5

ORIGINAL ARTICLE

Modeling the effect of dendritic input location on MEG and EEG source dipoles

Seppo P. Ahlfors[1,2] · **Christopher Wreh II**[1]

Received: 5 May 2014 / Accepted: 2 April 2015 / Published online: 12 April 2015

Abstract The cerebral sources of magneto- and electroencephalography (MEG, EEG) signals can be represented by current dipoles. We used computational modeling of realistically shaped passive-membrane dendritic trees of pyramidal cells from the human cerebral cortex to examine how the spatial distribution of the synaptic inputs affects the current dipole. The magnitude of the total dipole moment vector was found to be proportional to the vertical location of the synaptic input. The dipole moment had opposite directions for inputs above and below a reversal point located near the soma. Inclusion of shunting-type inhibition either suppressed or enhanced the current dipole, depending on whether the excitatory and inhibitory synapses were on the same or opposite side of the reversal point. Relating the properties of the macroscopic current dipoles to dendritic current distributions can help to provide means for interpreting MEG and EEG data in terms of synaptic connection patterns within cortical areas.

Keywords Magnetoencephalography · Electroencephalography · Postsynaptic current · Pyramidal cells

✉ Seppo P. Ahlfors
seppo@nmr.mgh.harvard.edu

[1] Athinoula A. Martinos Center for Biomedical Imaging, Massachusetts General Hospital/Harvard Medical School, 149 13th Street, Rm 2301, Charlestown, MA 02129, USA

[2] Harvard-MIT Division of Health Sciences and Technology, Cambridge, MA 02135, USA

1 Introduction

In electro- and magnetoencephalography (EEG, MEG), electrical activity in the brain is studied noninvasively by recording scalp potentials and extracranial magnetic fields, respectively (see, e.g., [64]). The sources of the EEG and MEG signals can be described as current dipoles, representing contributions from regional activity within the cerebral cortex [16, 65]. The relationship between the macroscopic current dipole and the underlying neural events is important for the interpretation of MEG and EEG data [20, 39, 50].

Biophysically based compartmental models have been used extensively to examine how the properties of the dendritic tree affect the somatic potential and thereby the firing patterns of individual cells [31, 33, 43, 54, 55, 61, 62, 66, 71]. Computational modeling can also provide valuable insights for understanding the neural origins of MEG and EEG [29, 30, 46–48] and other noninvasive recordings of brain activity [10, 13, 14, 28, 36, 42]. When modeling the neural currents generating the MEG and EEG signals, it is essential to take into account the orientation of the dendritic branch elements in 3D space, which is usually not required for modeling the somatic potential.

Spatially asymmetric currents, known as open-source configurations [40], are necessary to generate the far-field signal measured by MEG and EEG. The main structural asymmetry in the pyramidal cell models is along the trunk of the apical dendrite, oriented approximately perpendicular to the cortical surface. Previously, Murakami and Okada [47] demonstrated the importance of the dendrites in the generation of the current dipole by computing the dipole resulting from somatic stimulation of realistically shaped cortical cells. The current dipole also strongly depends on the spatial distribution of synaptic inputs within the dendrites [7]. Using reduced-complexity computational models for cortical

neurons in a network, Jones and colleagues found a reversal of the dipole direction in response to stimulation of basal versus distal apical dendrites, with the dynamics closely matching experimental somatosensory MEG data [29, 30]. In a computational model with realistic dendritic geometry of a layer-5 pyramidal cell from the cat visual cortex, Linden et al. [35] found that for low-frequency (1 Hz) inputs, the magnitude of the current dipole moment was approximately proportional to the distance from the soma. The objective of the present study was to determine whether a linear relationship between the dendritic input location and the macroscopically observable dipole moment can be found also in models of pyramidal cells from the human cerebral cortex.

2 Methods

2.1 Pyramidal cell models

Biophysically motivated computational models for human cortical pyramidal cells were constructed using the NEURON software [12, 24] (http://www.neuron.yale.edu). Dendritic geometries of the cells were obtained from the NeuroMorpho database (http://neuromorpho.org); axons were omitted. In total, 86 different cells were examined: *group I*: 36 layer-5 pyramidal cells from human anterior cingulate cortex (ACC) [70]; *group II*: 36 layer-3 magnopyramidal neurons from human inferior frontal gyrus (IFG, Brodmann area 45) [23]; *group III*: 14 layer-3 pyramidal cells from human infant superior frontal gyrus [68].

Passive membrane properties were assumed [25, 60]. The specific membrane capacitance was chosen to be $C_m = 1\ \mu F/cm^2$, the specific membrane resistance $R_m = 5000\ \Omega\ cm^2$, the equilibrium potential $V_{rest} = -75$ mV, and the specific intracellular (axial) resistivity $R_a = 80\ \Omega$ cm [63]. The value for R_m, was close to the value found for distal dendrites in a non-uniform model [63], but somewhat lower than what is commonly used in modeling studies (10^4–$10^5\ \Omega\ cm^2$).

The coordinate system was chosen such that the positive z-axis was aligned with the trunk of the apical dendrite in the proximal–distal direction and thus expected to be approximately perpendicular to the cortical surface for most pyramidal cells. The origin was at the soma, and the xy-plane was normal to the z-axis.

2.2 Synaptic input

Synaptic inputs were modeled as changes in the transmembrane conductivity g_{syn} [58] and were implemented using the NEURON software's point process mechanism. The synaptic transmembrane current was

$$I_{syn}(t) = g_{syn}(t)\left[V_{syn}(t) - E_{syn}\right], \tag{1}$$

where E_{syn} is the reversal potential for the synapse, $V_{syn}(t)$ is the transmembrane potential, and t is time. For excitatory synapses, we used $E_{syn} = 0$, and for shunt-type inhibitory synapses, $E_{syn} = V_{rest}$. The time course of the excitatory synaptic activation was assumed to have the form of the alpha function:

$$g_{syn}(t) = g_{max}\left[(t - t_0)/\tau_{syn}\right]\ \exp\left[1 - (t - t_0)/\tau_{syn}\right] \quad \text{for } t \geq t_0, \tag{2}$$

with the onset time t_0, time constant τ, and the amplitude scaling factor g_{max}; $g_{syn}(t) = 0$ for $t \leq t_0$. The maximum conductivity occurred at time $t_0 + \tau$. For excitatory synapses, we used $t_0 = 0$ ms, $\tau_{syn} = 0.7$ ms, and $g_{max} = 1$ nS, approximating the time course of AMPA-type receptor-mediated conductances [22]. When included, the shunting-type inhibitory synapses were assumed to be continuously active with $g_{syn}(t) = g_{max} = 10$ nS.

The locations of the synapses were chosen to match the node points within each dendritic segment, as determined by the d_lambda rule function in the NEURON software [12]. Synapses were placed throughout the model cells, with an average (±SD) distance between neighboring synapses being 11 ± 4 μm (group I), 16 ± 5 μm (group II), and 13 ± 5 μm (group III). Synapses were activated either individually or in groups involving all synapses within 100 μm in their z-coordinate ("z-bands").

2.3 Current dipole moment

Dendritic segments were assumed to be cylindrical (Fig. 1). Within a segment, the axial current vector is $\mathbf{I}_a = I_a\ \mathbf{e}_a$, where $\mathbf{e}_a = (\mathbf{r}_0 - \mathbf{r}_1)/L$ is a unit vector in the axial direction, $\mathbf{r}_0$ and $\mathbf{r}_1$ are the corresponding position vectors for the proximal and distal ends of the segment, and $L = \|\mathbf{r}_0 - \mathbf{r}_1\|$ is the length of the cylinder. The magnitude of the axial current is, according to Ohm's law, $I_a = (V_1 - V_0)/R = (V_1 - V_0)\ \pi\ d^2/(4\ R_a\ L)$, where V_0 and V_1 are the membrane voltages at the two ends of the segment, $R = R_a\ L/\pi\ (d/2)^2$ is the total resistance of that segment, R_a is the specific intracellular resistivity, and d is the diameter of the cylinder.

The current dipole moment vector $\mathbf{Q}$ for a dendritic cylinder was obtained by multiplying the intracellular axial current vector by the length of that segment [49, 69]:

$$\mathbf{Q} = \mathbf{I}_a L = \left[(V_1 - V_0)\pi d^2/(4R_a)\right]\mathbf{e}_a. \tag{3}$$

The NEURON software computed V_1 and V_0 for all segments of a model cell by solving the cable equation [24]. For each cell, the total current dipole was obtained as the vector sum of the dipole moments for all compartments [48]. We examined the dipole moment component

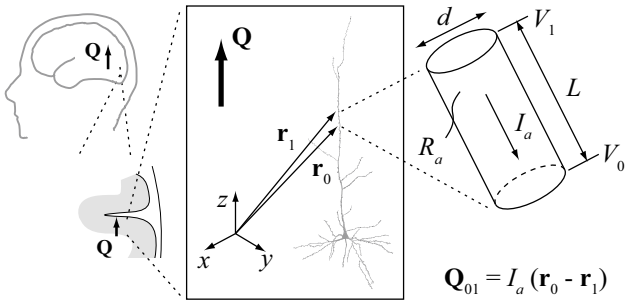

Fig. 1 Modeling the current dipole resulting from dendritic currents in a pyramidal cell. The total macroscopic current dipole **Q** (symbolized by the *thick arrow*) was computed as the sum of the dipole moment vectors calculated for cylindrical segments. L denotes the length and d the diameter of a single segment. The proximal and distal ends of the segment relative to the soma are labeled as "0" and "1", respectively. The position vectors of the end points are $\mathbf{r}_0 = (x_0, y_0, z_0)$ and $\mathbf{r}_1 = (x_1, y_1, z_1)$, and the transmembrane potentials are V_0 and V_1. R_a is the axial resistance of the intracellular fluid. The current dipole moment vector for this segment is $\mathbf{Q}_{01} = I_a\,(\mathbf{r}_0 - \mathbf{r}_1)$, cf. Eq. (3). The coordinate system was chosen such that the positive z-axis is aligned with the trunk of the apical dendrite, pointing upward; the xy-plane is normal to the z-axis. The positive direction of the axial current I_a is by convention toward the soma; thus, a positive I_a in the trunk of the apical dendrite results in a negative z-component Q_z of the current dipole

Q_z approximately perpendicular to the cortical surface; for symmetry reasons, the lateral dipole moment components are expected to cancel out in a large population of cells [40]. We were particularly interested in the sign of Q_z, which indicates whether the direction of the current dipole is toward or away from the white matter below the cortex.

The simulation time window was from 5 ms before to 35 ms after the onset of the excitatory input. The magnitudes of the response time courses were quantified by the time integrals (area under the curve), denoted by V_s^A and Q_z^A. For the latency, we used the centroid point [1]. A linear regression model was determined for the dependence of Q_z^A on the z-location of the synaptic input:

$$Q_z^A(z) = k_Q(z - z_0) + \varepsilon(V), \tag{4}$$

where z_0 indicates the input location where the direction (sign) of the current dipole vector reverses and $\varepsilon(z)$ is the residual error.

The transient excitatory synaptic conductivity change was always unidirectional (alpha function, Eq. 2), and we did not directly address the frequency dependence of the response (cf. [35, 52]). However, we examined the presence of sign reversals in the response time course of Q_z was identified with the help of a bidirectionality index

$$\beta = 1 - \left| \int Q_z(t)\mathrm{d}t \right| \Big/ \int |Q_z(t)\mathrm{d}t|. \tag{5}$$

If the response $Q_z(t)$ for a given input has the same sign for all time points t, then $\beta = 0$ (unidirectional); for equal amount of positive and negative values, $\beta = 1$ (maximally bidirectional).

3 Results

3.1 Current dipole in response to excitatory input at different dendritic locations

Figure 2a shows simulated time courses of the somatic potential V_s and the vertical component Q_z of the total current dipole moment in response to a single excitatory synaptic input at six different locations of a pyramidal cell model. The spatial distribution of the synaptic inputs influenced several types of qualitative dissociations between V_s and Q_z in terms of the magnitude, direction, and timing of the transient responses. The responses in V_s were largest for inputs at or near the soma, and the direction was always the same, i.e., depolarization for excitatory inputs. In contrast, the response in Q_z was largest with the most distal apical input. Furthermore, Q_z reversed its direction, being negative (dipole pointing downward, toward the white matter) for the apical input locations and positive for the soma and basal locations. The response magnitudes V_s^A and Q_z^A for individual synapses throughout the cell further illustrate the characteristic dependence on the input location (Fig. 2b). When plotted as a function of the z-coordinate of the synaptic input location, the data revealed that the sign of Q_z^A reversed at a small positive z-value near the soma (Fig. 2c). For this cell, a linear fit for Q_z^A gave $z_0 = 67$ µm above the soma for the reversal point and $k_Q = -1.1$ fAm ms/µm for the slope, with the coefficient of determination $r^2 = 0.988$. The latency of the response was shorter for Q_z^A than that for V_s^A for all input locations (Fig. 2d), consistent with the time courses of Q_z being more closely related to the time course of the local membrane potential and the postsynaptic currents near the site of the input than to those at the soma.

The response magnitudes V_s^A and Q_z^A as a function of the synapse location are illustrated in Fig. 3 for several individual cells from each group. The sign of Q_z^A reversed consistently near the soma in all these models.

Averaged data from the three groups of human cortical cell models are depicted in Fig. 4. The change in the somatic potential was always positive and largest for inputs proximal to the soma (Fig. 4a), whereas the magnitude of the dipole moment Q_z^A was proportional to the z-location of the synapse (Fig. 4b). Linear regression for Q_z^A gave the mean (±SD) values of $z_0 = 13 \pm 30$ µm, $k_Q = -1.2 \pm 0.2$ fAm/µm, $r^2 = 0.954 \pm 0.026$ (group I); $z_0 = 26 \pm 41$ µm, $k_Q = -1.1 \pm 0.06$ fAm/µm, $r^2 = 0.987 \pm 0.012$ (group II); and $z_0 = 40 \pm 24$ µm,

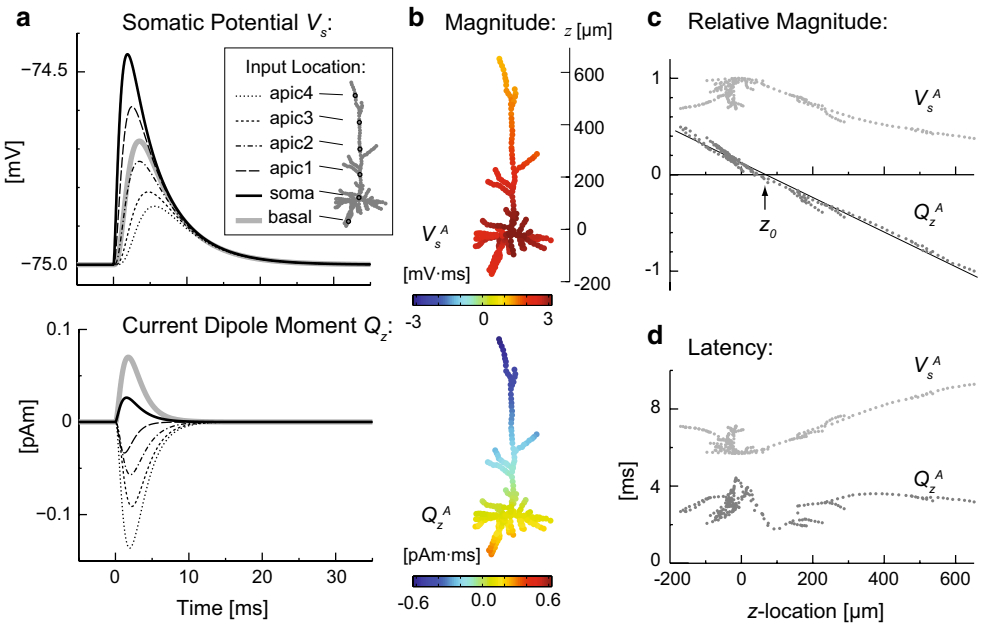

Fig. 2 Computed somatic potential (V_s) and the total current dipole moment in the z-direction (Q_z) in response to synaptic inputs at different locations of a pyramidal cell model. **a** Time courses of V_s (*top*) and Q_z (*bottom*). The excitatory input occurred at time "0 ms" at one of the six locations indicated in the *inset*. **b** Response magnitudes V_s^A and Q_z^A (*area under curve*) for all individual synaptic input locations for the same cell. The *scale on the right* indicates the vertical (z-) location relative to the soma. **c** Normalized values of V_s^A and Q_z^A as a function of the z-coordinate of the synaptic input location. V_s^A was largest when the input was at soma; Q_z^A showed near-linear dependence on the z-location of the input. The reversal point for the sign of Q_z^A, as determined by a linear fit, was $z_0 = 67$ µm. **d** The centroid point latency of V_s^A and Q_z^A. The latency of V_s^A was longer than the latency of Q_z^A for all input locations. The dendritic morphology of this cell model was from [70], labeled "04a_pyramidal4aACC" in the NeuroMorpho database

$k_Q = -1.3 \pm 0.08$ fAm/µm, $r^2 = 0.983 \pm 0.023$ (group III). The dendritic segments were not equally distributed across the z-bands: Most of the segments (and thus also the simulated input locations) were close to the soma (Fig. 4c). The sum of the current dipole magnitudes to all individual synaptic inputs within z-bands showed a step-function-like dependence on the input location (Fig. 4d). The smaller number of inputs in the most distal z-bands appeared to counteract the effect of the larger dipole moments for individual inputs at these locations. For all three groups of cell models, the mean values of the centroid latency for Q_z^A were systematically shorter than those for V_s^A and showed only weak dependence on the input location, similar to the single-cell results in Fig. 2d.

For all three groups of cell models, bidirectional responses were relatively rare and associated with low overall response amplitude. The mean percentage (±SD) of input locations for which the bidirectionality index $\beta > 0.1$ was 9.7 ± 7.1 % (group I), 4.0 ± 3.6 % (group II), and 5.6 ± 4.8 % (group III). The ratio of the largest value of the time integral of the absolute dipole moment magnitude $\left(\int |Q_z(t)|dt\right)$ among input locations for which $\beta > 0.1$ versus that among all input locations was 12 ± 9 % (group I), 4 ± 3 % (group II), and 10 ± 6 % (group III).

3.2 Combination of excitatory and inhibitory inputs

The effect of simultaneous excitatory and inhibitory synapses is illustrated in Fig. 5. When a shunting-type inhibitory synapse was located anywhere between the excitatory input and the soma, V_s^A was suppressed. The suppression of Q_z^A depended more strongly than that of V_s^A on the distance between the inhibitory and excitatory synapses (e.g., the case of "Excit: apic4," for inhibitory at "apic2" and "apic3" in Fig. 5a). When the inhibitory synapse was more distal than the excitatory one, there was relatively little suppression in V_s^A, but a strong suppression in Q_z^A ("Excit: apic2," for inhibitory at "apic3" and "apic4"). The combination of excitatory input at the soma or the basal dendrites and inhibitory input at apical locations resulted in an enhancement rather than suppression in Q_z^A ("Excit: soma," inhibitory at "apic1–4").

Figure 5b depicts average values of the relative change in V_s^A and Q_z^A for the 36 cell models of group I, when excitatory and inhibitory inputs were presented simultaneously within bands of the z-coordinate. Inhibitory synapses at or near the soma strongly suppressed V_s^A. In contrast, Q_z^A was suppressed more when the inhibitory synapses were located on the distal rather than proximal side (with respect to the reversal point z_0, which typically was close to the soma) of

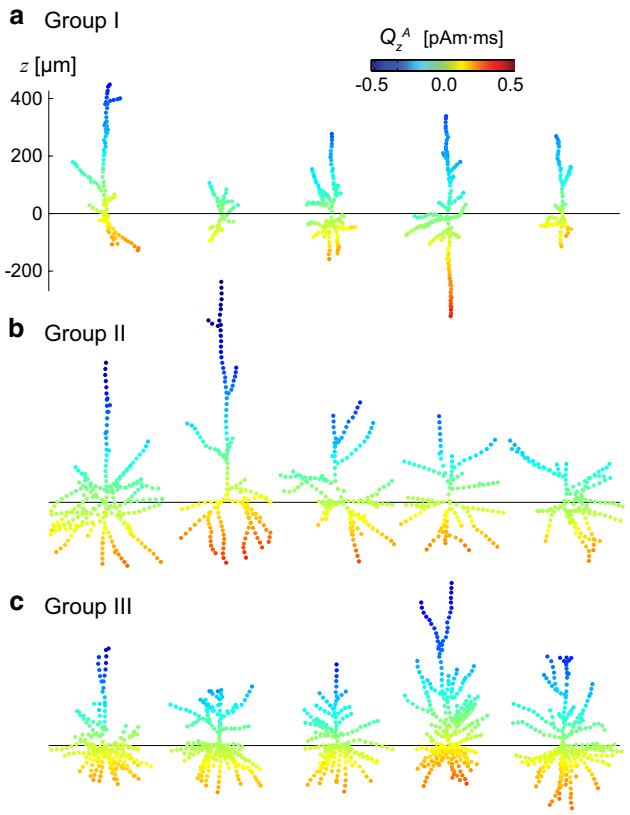

Fig. 3 Response magnitudes V_s^A and Q_z^A for cells from the three groups: **a** group I, **b** group II, and **c** group III. Five examples of cell geometries from each group were chosen to illustrate the structural variability among the cells. The *horizontal lines* indicate the location of the soma ($z = 0$) for each cell. The dependence of Q_z^A on the vertical location of the synaptic input shows a consistent pattern despite the varying dendritic architectures

the excitatory synapses. When the excitatory and inhibitory synapses were on the opposite sides of the reversal point z_0, Q_z^A was enhanced. This result can be understood in terms of the effective strength of the shunting-type inhibition being dependent on the local transmembrane potential, which is typically much larger on the distal than on the proximal side of an excitatory synapse [55], thereby enhancing the effect of distal inhibitory inputs on Q_z^A.

4 Discussion

The dependence of the total current dipole moment on the location of the synaptic input was examined in computational models of 86 human pyramidal cells from three different regions of the cerebral cortex. The vertical component of the dipole moment was found to be proportional to the vertical location of the synapse within the dendritic tree. The dipole moment had opposite directions for inputs above and below a reversal point close to the soma, inward (pointing toward white matter) for excitatory inputs for distal apical input locations, and outward for basal locations. The results are consistent with previous modeling studies based on a cat visual cortex pyramidal cell [35] as well as on a simplified dendritic geometry [7].

The dependence of the dipole moment on the input location was similar for the three groups of cells studied, in spite of the differences among the cells in the length and branching structure of the dendrites. The current dipole results from an asymmetric flow of postsynaptic axial currents. The likely contributors to the axial currents being larger toward the soma than away from it are the asymmetric distribution of dendritic diameters, viz larger diameters proximal to the soma provide a lower resistance for the axial current, and the sealed ends of the dendritic branches. All the cell models studied here shared these general features. Furthermore, the reversal point for the current dipole was not sensitive to the specific model parameters: Using the model with six input locations depicted in Fig. 2a as a test case, we varied the axial conductance, membrane resistance, membrane capacitance, and an overall scaling factor for the segment diameters in the range of 25–400 %, but in no case did a change in any of these parameters result in a reversal of the dipole moment direction.

The systematic dependence of the current dipole magnitude and direction between the spatial locations of synaptic inputs may allow experimentally observed MEG and EEG source dipoles to provide information about the distribution of synaptic input patterns across cortical layers. Since hierarchical organization between cortical areas is associated with specific laminar patterns of anatomical connections [8, 19, 57], it is conceivable that feedforward- and feedback-type inputs into a cortical area can result in different directions for the MEG and EEG source dipoles [5, 26, 30]. MEG and EEG are sensitive to the orientation of the source currents, and both the physical orientation and the physiological direction of the current dipole can in many cases be determined reliably [2, 3]. In particular, excitatory inputs to the apical tuft of pyramidal cells in the superficial cortical layers result in surface-negative EEG [15, 67], corresponding to current dipole direction toward the white matter. Multi-contact intracranial recordings can provide data about the expected dipole direction in terms of laminar input patterns and neural excitation [9, 21, 41, 45, 53, 59]. For the interpretation of the macroscopic current dipole in terms of the input type, however, it will be important to relate the laminar locations of the synaptic inputs to their locations within the dendritic tree of the individual neurons [51].

The dipole direction is affected not only by the spatial distribution of the synaptic inputs, but also by their excitatory versus inhibitory nature [6, 38]. For example, changing the synaptic reversal potential from excitatory to inhibitory

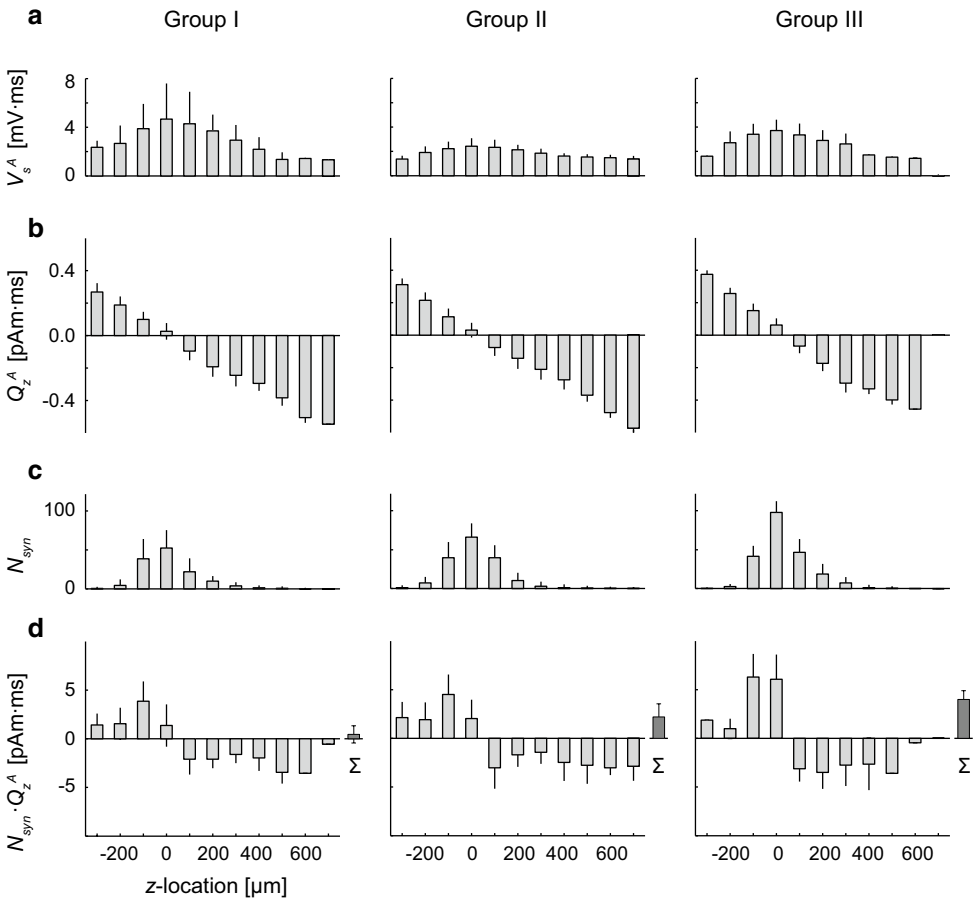

Fig. 4 Response magnitudes of the somatic potential V_s^A and the current dipole moment Q_z^A as a function of the vertical location of the synaptic input, averaged over multiple cell models. Group I: 36 layer-5 pyramidal cells from human anterior cingulate cortex [70]; group II: 36 layer-3 magnopyramidal neurons from human inferior frontal gyrus [23]; group III: 14 layer-3 pyramidal cells from human infant superior frontal gyrus [68]. Mean and standard deviation of **a** V_s^A, **b** Q_z^A, **c** the number of simulated synapses N_{syn} within 100-μm-wide bands of the z-coordinate, and **d** the total dipole moment Q_z^A weighted by N_{syn}. In (**d**), the *rightmost bar* (Σ) indicates the net dipole moment for the sum of responses to all input locations. For each individual cell model, the soma was at $z = 0$. The current dipole moment Q_z^A for individual synapses (**b**) showed approximately linear dependence on z for all three model groups. However, when the number of synapses was taken into account (**d**), the weighted dipole moment was more uniform across the z-bands

would reverse the sign of both V_{s} and Q_z. However, when excitatory and inhibitory synapses were combined, the response properties of V_{s} and Q_z showed notable differences. Shunting-type inhibition is known to prominently reduce V_{s} when placed between the excitatory inputs and the soma [32]. The magnitude of Q_z, however, was either suppressed or enhanced, depending on whether the excitatory and inhibitory inputs were on the same or on the opposite side of the location where the dipole moment to a single synapse was minimal (the reversal point z_0). Thus, the interpretation of the current dipole magnitude and direction in the presence of inhibitory inputs is challenging because of the combined effect of the type and the spatial distribution of the inputs.

In general, cancelation effects at various spatial scales can diminish the magnitude of far-field signals such as the MEG and EEG. For example, cancelation of MEG and EEG signals may occur due to cortical folding when there are source currents in opposing sulcal walls [4, 27]. Substantial cancelation also takes place locally, both within individual cells and in cell populations. In individual cells, as examined here, contributions from axial currents of opposite directions will partially cancel in the computation of the current dipole moment. An example of complete cancelation of this type is the vanishing of the dipole moment when the synaptic input is at the reversal point. For local cell populations, cancelation in the total current dipole will occur when the dipoles for individual cells have opposite directions, for example, if sets of excitatory inputs simultaneously connect to the basal dendrites of one subpopulation and to the apical dendrites of another.

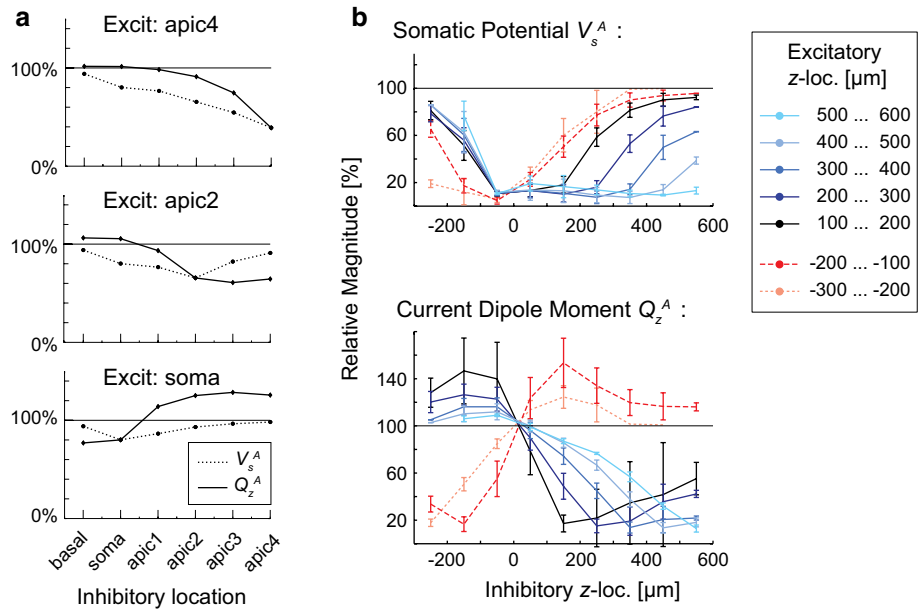

Fig. 5 Response magnitudes V_s^A and Q_z^A for combined excitatory and inhibitory inputs. **a** Relative magnitudes, compared with the excitatory-only case (=100 %), for pairs of individual synapses in the single-cell model shown in Fig. 2. *Each panel* corresponds to one location of excitatory input (apic4, apic2, or soma) with a shunting-type inhibitory synapse at one of six locations (basal, soma, apic1–4). V_s^A and Q_z^A showed different dependence on the relative location of the excitatory and inhibitory synapses. **b** Average normalized magnitude of V_s^A and Q_z^A for the combinations of excitatory and inhibitory inputs within 100-µm bands of z-location in the 36 cell models of group I (100 % = excitatory only). Again, prominent differences between V_s^A and Q_z^A dependent on the relative location of excitatory and inhibitory inputs were seen. For example, the inclusion of inhibitory inputs always suppressed V_s^A, particularly when the inhibitory synapses were near the reversal point, which was typically close to the soma. In contrast, the inhibitory inputs could either suppress or enhance Q_z^A. Enhancement of Q_z^A was seen when excitatory and inhibitory synapses were on the opposite sides of the soma

For sinusoidal inputs, the total current dipole moment is suppressed because of phase delays among the axial currents within the dendritic tree [35]. Computational modeling studies of the local field potential (LFP) have demonstrated how the current dipole representing the source of far-field LFP (and also of MEG and scalp EEG) has temporal low-pass filtering characteristics due to the dendritic tree [34, 35, 52]. In the present study, the response waveforms for Q_z to transient unidirectional excitatory inputs were mostly unidirectional, except for inputs located near the reversal point z_0. Suppression of the current dipole moment for biphasic responses to repeated inputs can occur, for example, if a late reversed-sign part of the response coincides with the early part of the response to a subsequent input. For the cell models studied here, however, when the responses were bidirectional, the overall magnitude of the dipole moment was found to be small and therefore expected to contribute only little to the observability of macroscopic current dipoles.

Restricting to the passive cell membrane model allowed us to simplify the exploration of the effects of the spatial distribution of synaptic inputs within the dendrites. However, active membrane properties are of major importance to dendritic function [37, 44] and are likely to have important contributions to LFP as well as MEG and EEG [47, 56]. Evidence for the importance of complex dendritic processing is accumulating, with dendritic segments being considered as computational units [11]. Furthermore, the dynamics within populations of neurons contributing to the net current dipole is of essential importance [17, 18, 30]. It would be of interest in future work to apply computational biophysical modeling to examine the effects of spatial distribution of synaptic inputs within subsets of dendritic branches associated with specific computational functions, combined with active membrane models and networks of neurons, to further illuminate the neural origins of MEG and EEG.

5 Conclusions

The compartmental biophysical models of human pyramidal cells suggested a linear relationship between the vertical location of the synaptic input and the corresponding current dipole moment. This relation may help to provide means to interpret MEG and EEG source estimates in terms of specific synaptic connection patterns within cortical areas.

Acknowledgments This work was supported by National Institutes of Health Grants NS57500 and NS037462, and by The National Center for Research Resources (P41RR14075).

References

1. Agmon-Snir H, Segev I (1993) Signal delay and input synchronization in passive dendritic structures. J Neurophysiol 70(5):2066–2085
2. Ahlfors SP, Hämäläinen MS (2012) MEG and EEG: Source estimation. In: Brette R, Destexhe A (eds) Handbook of neural activity measurement. Cambridge University Press, Cambridge, pp 257–286
3. Ahlfors SP, Han J, Belliveau JW, Hämäläinen MS (2010) Sensitivity of MEG and EEG to source orientation. Brain Topogr 23(3):227–232. doi:10.1007/s10548-010-0154-x
4. Ahlfors SP, Han J, Lin FH, Witzel T, Belliveau JW, Hämäläinen MS, Halgren E (2010) Cancellation of EEG and MEG signals generated by extended and distributed sources. Hum Brain Mapp 31(1):140–149. doi:10.1002/hbm.20851
5. Ahlfors SP, Jones SR, Ahveninen J, Hämäläinen MS, Belliveau JW, Bar M (2015) Direction of magnetoencephalography sources associated with feedback and feedforward contributions in a visual object recognition task. Neurosci Lett 585:149–154. doi:10.1016/j.neulet.2014.11.029
6. Allison T, Puce A, McCarthy G (2002) Category-sensitive excitatory and inhibitory processes in human extrastriate cortex. J Neurophysiol 88(5):2864–2868
7. Avitan L, Teicher M, Abeles M (2009) EEG generator–a model of potentials in a volume conductor. J Neurophysiol 102(5):3046–3059. doi:10.1152/jn.91143.2008
8. Barbas H, Zikopoulos B (2007) The prefrontal cortex and flexible behavior. Neuroscientist 13(5):532–545. doi:10.1177/1073858407301369
9. Barth DS, Sutherling W (1988) Current source-density and neuromagnetic analysis of the direct cortical response in rat cortex. Brain Res 450(1–2):280–294
10. Blagoev KB, Mihaila B, Travis BJ, Alexandrov LB, Bishop AR, Ranken D, Posse S, Gasparovic C, Mayer A, Aine CJ, Ulbert I, Morita M, Muller W, Connor J, Halgren E (2007) Modelling the magnetic signature of neuronal tissue. Neuroimage 37(1):137–148
11. Branco T, Hausser M (2010) The single dendritic branch as a fundamental functional unit in the nervous system. Curr Opin Neurobiol 20(4):494–502
12. Carnevale NT, Hines ML (2005) The NEURON Book. Cambridge University Press, Cambridge
13. Cassara AM, Hagberg GE, Bianciardi M, Migliore M, Maraviglia B (2008) Realistic simulations of neuronal activity: a contribution to the debate on direct detection of neuronal currents by MRI. Neuroimage 39(1):87–106
14. Cassara AM, Maraviglia B, Hartwig S, Trahms L, Burghoff M (2009) Neuronal current detection with low-field magnetic resonance: simulations and methods. Magn Reson Imaging 27(8):1131–1139
15. Cauller L (1995) Layer I of primary sensory neocortex: where top-down converges upon bottom-up. Behav Brain Res 71(1–2):163–170
16. Cohen D, Halgren E (2003) Magnetoencephalography (Neuromagnetism). In: Adelman G, Smith BH (eds) Encyclopedia of neuroscience, vol II, 3rd edn. Elsevier, Amsterdam
17. David O, Friston KJ (2003) A neural mass model for MEG/EEG: coupling and neuronal dynamics. Neuroimage 20(3):1743–1755
18. Deco G, Jirsa VK, Robinson PA, Breakspear M, Friston K (2008) The dynamic brain: from spiking neurons to neural masses and cortical fields. PLoS Comput Biol 4(8):e1000092
19. Felleman DJ, Van Essen DC (1991) Distributed hierarchical processing in the primate cerebral cortex. Cereb Cortex 1(1):1–47
20. Gonzalez Andino SL, Perrig S, de Peralta Grave, Menendez R (2011) Spatiotemporal scales and links between electrical neuroimaging modalities. Med Biol Eng Comput 49(5):511–520. doi:10.1007/s11517-011-0769-4
21. Halgren E, Wang C, Schomer DL, Knake S, Marinkovic K, Wu J, Ulbert I (2006) Processing stages underlying word recognition in the anteroventral temporal lobe. Neuroimage 30(4):1401–1413. doi:10.1016/j.neuroimage.2005.10.053
22. Hausser M, Roth A (1997) Estimating the time course of the excitatory synaptic conductance in neocortical pyramidal cells using a novel voltage jump method. J Neurosci 17(20):7606–7625
23. Hayes TL, Lewis DA (1996) Magnopyramidal neurons in the anterior motor speech region. Dendritic features and interhemispheric comparisons. Arch Neurol 53(12):1277–1283
24. Hines ML, Carnevale NT (1997) The NEURON simulation environment. Neural Comput 9(6):1179–1209
25. Holmes WR (2010) Passive Cable Modeling. In: De Schutter E (ed) Computational modeling methods for neuroscientists. MIT Press, Cambridge, pp 233–258
26. Inui K, Kakigi R (2006) Temporal analysis of the flow from V1 to the extrastriate cortex in humans. J Neurophysiol 96(2):775–784
27. Irimia A, Van Horn JD, Halgren E (2012) Source cancellation profiles of electroencephalography and magnetoencephalography. Neuroimage 59(3):2464–2474. doi:10.1016/j.neuroimage.2011.08.104
28. Jay WI, Wijesinghe RS, Dolasinski BD, Roth BJ (2012) Is it possible to detect dendrite currents using presently available magnetic resonance imaging techniques? Med Biol Eng Comput 50(7):651–657. doi:10.1007/s11517-012-0899-3
29. Jones SR, Pritchett DL, Sikora MA, Stufflebeam SM, Hämäläinen M, Moore CI (2009) Quantitative analysis and biophysically realistic neural modeling of the MEG mu rhythm: rhythmogenesis and modulation of sensory-evoked responses. J Neurophysiol 102(6):3554–3572. doi:10.1152/jn.00535.2009
30. Jones SR, Pritchett DL, Stufflebeam SM, Hämäläinen M, Moore CI (2007) Neural correlates of tactile detection: a combined magnetoencephalography and biophysically based computational modeling study. J Neurosci 27(40):10751–10764. doi:10.1523/JNEUROSCI.0482-07.2007
31. Koch C (1999) Biophysics of computation: information processing in single neurons. Oxford University Press, New York
32. Koch C, Poggio T, Torre V (1983) Nonlinear interactions in a dendritic tree: localization, timing, and role in information processing. Proc Natl Acad Sci USA 80(9):2799–2802
33. Korogod SM, Tyc-Dumont S (2009) Electrical dynamics of the dendritic space. Cambridge University Press, Cambridge
34. Leski S, Linden H, Tetzlaff T, Pettersen KH, Einevoll GT (2013) Frequency dependence of signal power and spatial reach of the local field potential. PLoS Comput Biol 9(7):e1003137. doi:10.1371/journal.pcbi.1003137PCOMPBIOL-D-13-00299
35. Linden H, Pettersen KH, Einevoll GT (2010) Intrinsic dendritic filtering gives low-pass power spectra of local field potentials. J Comput Neurosci 29(3):423–444. doi:10.1007/s10827-010-0245-4
36. Liston A, Bayford R, Holder D (2012) A cable theory based biophysical model of resistance change in crab peripheral nerve and human cerebral cortex during neuronal depolarisation: implications for electrical impedance tomography of fast neural activity in the brain. Med Biol Eng Comput 50(5):425–437. doi:10.1007/s11517-012-0901-0
37. Llinas RR (1988) The intrinsic electrophysiological properties of mammalian neurons: insights into central nervous system function. Science 242(4886):1654–1664

38. Lopes da Silva F, Van Rotterdam A (1993) Biophysical aspects of EEG and magnetoencephalogram generation. In: Niedermeyer E, Lopes da Silva F (eds) Electroencephalography: basic principles, clinical applications, and related fields, 3rd edn. Lippincott, Williams and Wilkins, Philadelphia, pp 78–91
39. Lopes da Silva FH (2010) Electrophysiological basis of MEG signals. In: Hansen P, Kringelbach M, Salmelin R (eds) MEG: an introduction to methods. Oxford University Press, New York, pp 1–23
40. Lorente de No R (1947) Action potential of the motoneurons of the hypoglossus nucleus. J Cell Physiol 29(3):207–287
41. Lu ZL, Williamson SJ (1991) Spatial extent of coherent sensory-evoked cortical activity. Exp Brain Res 84(2):411–416
42. Luo Q, Jiang X, Chen B, Zhu Y, Gao JH (2011) Modeling neuronal current MRI signal with human neuron. Magn Reson Med 65(6):1680–1689. doi:10.1002/mrm.22764
43. Mainen ZF, Sejnowski TJ (1996) Influence of dendritic structure on firing pattern in model neocortical neurons. Nature 382(6589):363–366. doi:10.1038/382363a0
44. Migliore M, Shepherd GM (2002) Emerging rules for the distributions of active dendritic conductances. Nat Rev Neurosci 3(5):362–370
45. Mitzdorf U (1985) Current source-density method and application in cat cerebral cortex: investigation of evoked potentials and EEG phenomena. Physiol Rev 65(1):37–100
46. Murakami S, Hirose A, Okada YC (2003) Contribution of ionic currents to magnetoencephalography (MEG) and electroencephalography (EEG) signals generated by guinea-pig CA3 slices. J Physiol 553:975–985
47. Murakami S, Okada Y (2006) Contributions of principal neocortical neurons to magnetoencephalography and electroencephalography signals. J Physiol 575(Pt 3):925–936. doi:10.1113/jphysiol.2006.105379
48. Murakami S, Zhang T, Hirose A, Okada YC (2002) Physiological origins of evoked magnetic fields and extracellular field potentials produced by guinea-pig CA3 hippocampal slices. J Physiol 544:237–251
49. Nunez P (1995) Neocortical dynamics and human EEG rhythms. Oxford University Press, New York
50. Okada YC, Wu J, Kyuhou S (1997) Genesis of MEG signals in a mammalian CNS structure. Electroencephalogr Clin Neurophysiol 103(4):474–485
51. Petreanu L, Mao T, Sternson SM, Svoboda K (2009) The subcellular organization of neocortical excitatory connections. Nature 457(7233):1142–1145
52. Pettersen KH, Einevoll GT (2008) Amplitude variability and extracellular low-pass filtering of neuronal spikes. Biophys J 94(3):784–802. doi:10.1529/biophysj.107.111179
53. Peyrache A, Dehghani N, Eskandar EN, Madsen JR, Anderson WS, Donoghue JA, Hochberg LR, Halgren E, Cash SS, Destexhe A (2012) Spatiotemporal dynamics of neocortical excitation and inhibition during human sleep. Proc Natl Acad Sci USA 109(5):1731–1736
54. Rall W, Agmon-Snir H (1998) Cable Theory for Dendritic Neurons. In: Koch C, Segev I (eds) Methods in neuronal modeling, 2nd edn. MIT Press, Cambridge, pp 27–92
55. Rall W, Rinzel J (1973) Branch input resistance and steady attenuation for input to one branch of a dendritic neuron model. Biophys J 13(7):648–687. doi:10.1016/S0006-3495(73)86014-X
56. Reimann MW, Anastassiou CA, Perin R, Hill SL, Markram H, Koch C (2013) A biophysically detailed model of neocortical local field potentials predicts the critical role of active membrane currents. Neuron 79(2):375–390. doi:10.1016/j.neuron.2013.05.023
57. Rockland KS, Pandya DN (1979) Laminar origins and terminations of cortical connections of the occipital lobe in the rhesus monkey. Brain Res 179(1):3–20
58. Roth A, van Rossum MCW (2010) Modeling Synapses. In: De Schutter E (ed) Computational modeling methods for neuroscientists. MIT Press, Cambridge, pp 139–159
59. Schroeder CE, Foxe JJ (2002) The timing and laminar profile of converging inputs to multisensory areas of the macaque neocortex. Brain Res Cogn Brain Res 14(1):187–198
60. Segev I, Burke RE (1998) Compartmental Models of Complex Neurons. In: Koch C, Segev I (eds) Methods in neuronal modeling, 2nd edn. MIT Press, Cambridge, pp 93–136
61. Segev I, London M (2000) Untangling dendrites with quantitative models. Science 290(5492):744–750
62. Spruston N (2008) Pyramidal neurons: dendritic structure and synaptic integration. Nat Rev Neurosci 9(3):206–221
63. Stuart G, Spruston N (1998) Determinants of voltage attenuation in neocortical pyramidal neuron dendrites. J Neurosci 18(10):3501–3510
64. Supek S, Magjarevic R (2011) Neurodynamic measures of functional connectivity and cognition. Med Biol Eng Comput 49(5):507–509. doi:10.1007/s11517-011-0779-2
65. van Oosterom A (2012) The inverse problem of bioelectricity: an evaluation. Med Biol Eng Comput 50(9):891–902. doi:10.1007/s11517-012-0941-5
66. van Ooyen A, Duijnhouwer J, Remme MW, van Pelt J (2002) The effect of dendritic topology on firing patterns in model neurons. Network 13(3):311–325
67. Vaughan HG Jr (1982) The neural origins of human event-related potentials. Ann NY Acad Sci 388:125–138
68. Vuksic M, Petanjek Z, Rasin MR, Kostovic I (2002) Perinatal growth of prefrontal layer III pyramids in Down syndrome. Pediatr Neurol 27(1):36–38
69. Vvedenskii VL, Hari R, Ilmoniemi R, Reinikainen K (1985) Physical basis of the generation of neuromagnetic fields. Biofizika 30(1):154–158
70. Watson KK, Jones TK, Allman JM (2006) Dendritic architecture of the von Economo neurons. Neuroscience 141(3):1107–1112
71. Williams SR, Stuart GJ (2003) Role of dendritic synapse location in the control of action potential output. Trends Neurosci 26(3):147–154